CHEMISTRY OF MATERIALS

Article

pubs.acs.org/cm

In Situ Probing of Stack-Templated Growth of Ultrathin $Cu_{2-x}S$ Nanosheets

Ward van der Stam,[†] Freddy T. Rabouw,[†] Jaco J. Geuchies,[†] Anne C. Berends,[†] Stijn O. M. Hinterding,[†] Robin G. Geitenbeek,[†] Joost van der Lit,[†] Sylvain Prévost,[‡] Andrei V. Petukhov,[§,∥] and Celso de Mello Donega*[,†]

[†]Condensed Matter and Interfaces, Debye Institute for Nanomaterials Science, Utrecht University, Post Office Box 80000, 3508 TA Utrecht, The Netherlands

[‡]Beamline ID02, European Synchrotron Radiation Facility, 71 avenue des Martyrs, 38000 Grenoble, France

[§]Physical and Colloid Chemistry, Debye Institute for Nanomaterials Science, Utrecht University, Padualaan 8, 3584 CH Utrecht, The Netherlands

[∥]Laboratory of Physical Chemistry, Department of Chemical Engineering and Chemistry, Eindhoven University of Technology, Post Office Box 513, 5600 MB Eindhoven, The Netherlands

Supporting Information

ABSTRACT: Ultrathin two-dimensional (2D) nanomaterials have attracted intense research efforts due to their extraordinary optoelectronic properties. However, the nucleation and growth mechanisms of 2D colloidal nanosheets are still poorly understood. Here, we follow the formation of ultrathin colloidal $Cu_{2-x}S$ nanosheets by in situ small-angle X-ray scattering. While thermal decomposition of copper−dodecanethiolates produces spheroidal $Cu_{2-x}S$ nanocrystals, the addition of chloride to the reaction mixture results in 2 nm thick $Cu_{2-x}S$ nanosheets with well-defined shape and size. Our results show that chloride stabilizes stacks of lamellar copper−thiolate supramolecular complexes, so that they remain intact beyond the onset of $Cu_{2-x}S$ nucleation at 230 °C, leading to 2D-constrained stack-templated nucleation and growth. The face-to-face stacking of the nanosheets reinforces the 2D constraints imposed by the lamellar soft template, since it prevents internanosheet mass transport and nanosheet coalescence, thereby inhibiting growth in the thickness direction and allowing only for lateral growth. Our work thus provides novel insights into soft-templating formation mechanisms of ultrathin colloidal nanosheets, which may be exploited for other metal sulfide compositions.

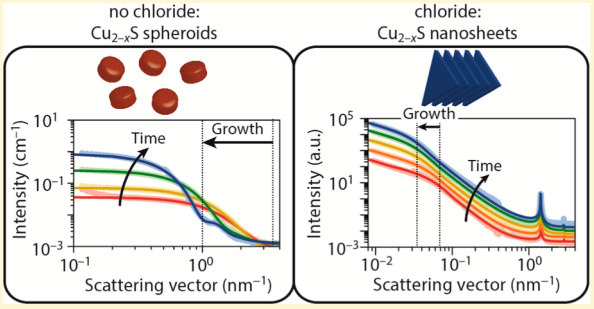

INTRODUCTION

The electronic properties of colloidal nanocrystals (NC) depend not only on their chemical composition but also on their size and shape.[1] By proper choice of reaction conditions and chemicals used in the synthesis, different sizes and shapes can be obtained, ranging from zero-dimensional (0D) quantum dots[2] to one-dimensional (1D) nanorods[3] and two-dimensional (2D) nanosheets.[4] Ultrathin 2D nanosheets (NS) possess extraordinary properties that are attractive for both fundamental studies and technological devices.[4−8] To date, colloidal nanosheets of a variety of compositions have been prepared (e.g., CdX with X = S, Se, Te;[9] PbS;[10,11] SnX, with X = S, Se;[12,13] In_2S_3;[14] $Cu_{2-x}S$;[15,16] $Cu_{2-x}Se$;[6] and WS_2[17]), but their formation mechanisms are still under debate. For example, the formation of PbS nanosheets has been attributed by Weller and co-workers[10] to oriented attachment of small PbS nanocrystals, while Buhro and co-workers[11] presented a mechanism in which the assembly of PbS NC building blocks is directed by lamellar mesophase templates. Soft-template mechanisms have also been invoked to explain the formation of CdX (X = S, Se) nanosheets, either by self-assembly of $(CdX)_n$ magic-size clusters within 2D lamellar templates[19−21] or by 2D constrained growth within soft templates formed by close packing of fatty acid chains.[18] However, the growth of ultrathin CdX (X = S, Se) nanosheets has also been explained by monomer addition to $(CdX)_n$ magic-size cluster seeds without templating effects.[9]

The controversy regarding the mechanisms that govern the formation of ultrathin colloidal nanosheets reflects the chemical diversity and complexity of the processes involved and cannot be resolved without in situ studies, which are nevertheless still lacking. In situ techniques are particularly effective in elucidating growth mechanisms, since they allow for real-time probing of all chemical processes involved, from the precursors to the final products. In situ transmission electron microscopy (TEM), powder X-ray diffraction (PXRD), and small-angle X-

Received: July 8, 2016
Revised: August 10, 2016
Published: August 11, 2016

DOI: 10.1021/acs.chemmater.6b02787
Chem. Mater. 2016, 28, 6381−6389

ray scattering (SAXS) have emerged as promising techniques to probe the nucleation and growth of nanomaterials. Liquid cell TEM is a direct-space imaging technique that can record the growth of individual (or a few) nanocrystals and has, for example, been used to analyze the formation of Pt and Pt_3Fe nanoparticles.[22,23] In situ PXRD can provide a more statistical picture of nanocrystal growth by probing an entire ensemble. It is sensitive to the nucleation, transformation, and growth of crystalline domains and has been used to follow the growth of spherical $Cu_{2-x}S$ nanocrystals[24] and TiO_2 nanoparticles.[25] In situ SAXS provides access to statistically averaged structural information on the superatomic scale and is especially suitable for studying the size and shape of nanoparticles and their self-organization into larger superstructures.[26] As will be shown, this makes it the technique of choice to elucidate the growth mechanism of ultrathin colloidal nanosheets. Nevertheless, high-temperature in situ SAXS studies of nucleation and growth of colloidal nanocrystals have been, until now, limited to spherical nanocrystals,[27] although the technique has been applied to study room-temperature formation of GeO_2 nanosheets within 2D lamellar interfacial phases[28] and stress-driven self-organization of oleic acid capped PbS nanocrystals into single-crystal nanosheets under high-pressure and solvent-free conditions.[29]

In this work, we follow the formation of both colloidal spheroidal $Cu_{2-x}S$ nanocrystals and colloidal ultrathin 2D $Cu_{2-x}S$ nanosheets in real time by performing in situ SAXS experiments. Both syntheses are based on thermal decomposition of copper−thiolate complexes, but the addition of chloride ions results in ultrathin $Cu_{2-x}S$ nanosheets with well-defined shape (triangular) and size (thickness 2 nm, lateral dimensions ∼110 nm, aspect ratio 55) rather than quasi-spherical $Cu_{2-x}S$ nanocrystals.[15] Our results show that copper−thiolate complexes form lamellar stacks that are thermally stabilized by bonds with chloride ions in solution, so that they remain structurally intact up to the onset of $Cu_{2-x}S$ nucleation at 230 °C, leading to 2D stack-templated nucleation and growth. Face-to-face stacking of the nanosheets inhibits growth in the thickness direction and allows only for lateral growth, resulting in large aspect ratios and constant thicknesses. Our work unravels the stack-templated formation mechanism that governs nucleation and growth of ultrathin colloidal 2D $Cu_{2-x}S$ nanosheets and adds another possibility to the vast library of soft-templating synthetic protocols that result in formation of self-standing colloidal ultrathin 2D nanomaterials.

EXPERIMENTAL SECTION

Materials. Copper(I) acetate [Cu(OAc), 97%], copper(I) chloride (CuCl, 97%), 1-dodecanethiol (DDT, ≥98%), 1-octadecene (ODE, tech., 90%), trioctylphosphine oxide (TOPO, 99%), anhydrous toluene, methanol, and butanol, were purchased from Sigma−Aldrich. All chemicals were used without any further purification.

Spheroidal $Cu_{2-x}S$ Nanocrystals. Spheroidal $Cu_{2-x}S$ nanocrystals were synthesized according to our previously reported method.[15] Typically, a stock solution was prepared, which contained 27.3 mg (0.22 mmol) of Cu(OAc), 0.55 g (1.42 mmol) of TOPO, and 0.5 mL (2.1 mmol) of DDT, dispersed in 12.5 mL of ODE. A small portion of this mixture was loaded in a 1 mm capillary and mounted in a Linkam heating stage. The capillary was rapidly heated to 230 °C at a heating rate of 80 °C/min. The reaction was maintained at this temperature for 60 min. The final $Cu_{2-x}S$ nanocrystals were removed from the capillary and precipitated by adding a methanol/butanol mixture, followed by centrifugation at 3000 rpm for 15 min. Afterward, the nanocrystals were redispersed in toluene.

Ultrathin $Cu_{2-x}S$ Nanosheets. Ultrathin $Cu_{2-x}S$ nanosheets were synthesized in the same way as described for spheroidal $Cu_{2-x}S$ nanocrystals, with the sole difference that Cu(OAc) was replaced by CuCl in the stock solution.

Small- and Wide-Angle X-ray Scattering Experiments. Small- and wide-angle X-ray scattering (SAXS and WAXS) experiments were performed at the ID02 beamline, European Synchroton Radiation Facility, Grenoble, France. The SAXS detector was a Rayonix MX-170HS mounted on a rail inside a vacuum chamber, which allowed us to probe the entire q range from 10^{-3} to 6 nm^{-1}. The wavelength of the collimated X-ray beam was 0.1 nm (12.4 keV). The WAXS detector was a Rayonix LX-170HS mounted on the beginning of the SAXS vacuum tube (calibrated with α-Al_2O_3) (see also Supporting Information, Figure S1).

Transmission Electron Microscopy. TEM images were acquired on a FEI Tecnai-10 microscope operating at 100 kV. Samples for TEM imaging were prepared by drop-casting a toluene solution of nanocrystals onto a carbon-coated copper (400-mesh) TEM grid.

Powder X-ray Diffraction. PXRD measurements were performed with a PW 1729 Philips diffractometer, equipped with a Cu Kα X-ray source (λ = 1.5418 Å). Samples for XRD analysis were prepared by depositing a concentrated solution of purified nanosheets in chloroform on a Si(100) substrate.

RESULTS AND DISCUSSION

Formation of $Cu_{2-x}S$ Nanocrystals Followed by in Situ Small-Angle X-ray Scattering. $Cu_{2-x}S$ nanocrystals were prepared by thermolysis of copper−dodecanethiolate single-source precursors at 230 °C in octadecene in the presence of trioctylphosphine oxide (see Experimental Section for details). In a typical experiment, the reaction mixture was loaded in a 1 mm diameter quartz capillary and mounted in a Linkam heating stage. The mixture was then heated to 230 °C at a rate of 80 °C/min and kept at the final temperature for ∼30 min, after which the nanocrystals were isolated and analyzed ex situ with TEM. The setup has a variable distance between sample and SAXS detector located in a vacuum tube. In this way, scattering could be recorded over a range of scattering vectors q from 10^{-3} to 6 nm^{-1} (Supporting Information, Figure S1). Such a large range is necessary to capture scattering from stacks of nanosheets or lamellar precursors separated by a few nanometers (large q)[15,30] as well as form-factor scattering due to the >100 nm lateral dimensions of the nanosheets (small q).[26,31] Each experiment was performed in triplicate, at three different detector-to-sample distances (Figure S1). The scattering signal was recorded by a 2D SAXS detector, and after azimuthal integration, a 1D scattering curve is obtained that covers the entire q-space (Figure 1b,e).

The final products formed in the capillaries were isolated and imaged by TEM (Figure 1a,d). The NC sizes and shapes obtained from the reaction in the capillaries (with only convective mixing and inhomogeneous heating, under air) closely match the morphologies obtained in larger-scale reactions under optimized conditions (13 mL volumes, under stirring, homogeneous heating, under N_2 atmosphere):[15] spheroidal nanocrystals in the absence of chlorides (Figure 1a) and ultrathin (2 nm thick) triangular nanosheets in the presence of chlorides (Figure 1d). This indicates that the NC formation studied here is robust to changes in reaction conditions and is therefore ideally suited for in situ X-ray scattering measurements. Furthermore, the crystallinity of the $Cu_{2-x}S$ nanosheets formed in situ is evident from X-ray scattering at wide angles (Supporting Information, Figure S2), which shows the same scattering peak observed in ex situ powder XRD experiments (d spacing = 1.95 Å), which

DOI: 10.1021/acs.chemmater.6b02787
Chem. Mater. 2016, 28, 6381−6389

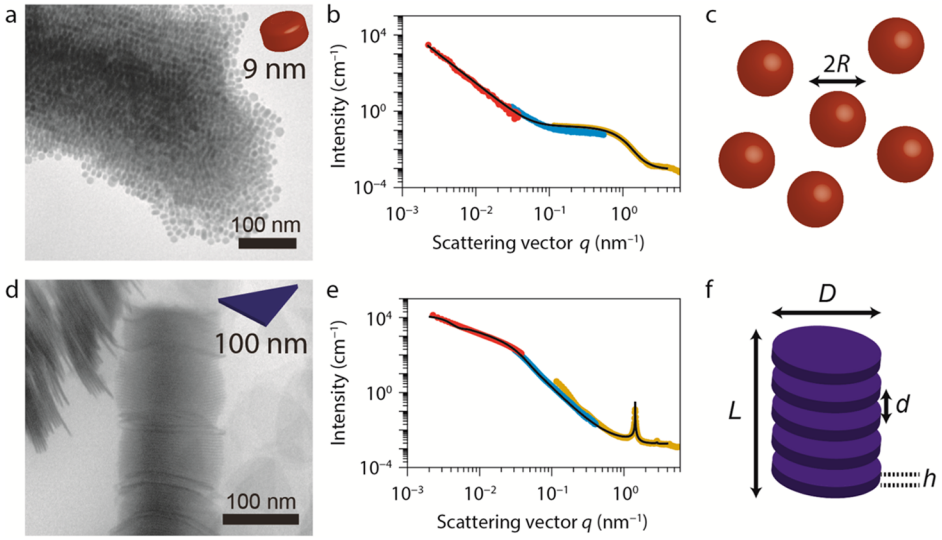

Figure 1. Representative TEM image and SAXS pattern for (a–c) spheroidal $Cu_{2-x}S$ nanocrystals and (d–f) ultrathin $Cu_{2-x}S$ nanosheets. (a) TEM image of spheroidal $Cu_{2-x}S$ nanocrystals obtained in a capillary when a reaction solution containing CuOAc, TOPO, and DDT in ODE was heated to 230 °C for 30 min. (b) In situ SAXS pattern of NC reaction mixture after 12 min at 230 °C, measured at three detector-to-sample distances (yellow, 1 m; blue, 5.5 m; red, 30 m). The black line shows the fit (see Supporting Information, Method 2). (c) Schematic of NC dimensions used in the model. (d) TEM image of ultrathin $Cu_{2-x}S$ nanosheets obtained in a capillary when a solution of CuCl, TOPO, and DDT in ODE was heated to 230 °C for 30 min. (e) In situ SAXS pattern of NS reaction mixture after 12 min at 230 °C, measured at three detector-to-sample distances (yellow, 1 m; blue, 5.5 m; red, 30 m). The black line shows the fit (see Supporting Information, Method 1). (f) Schematic of NS and NS stack dimensions used in the model (see Supporting Information, Method 1 and Figure S3).

corresponds to a tetragonal polymorph of the digenite ($Cu_{1.8}S$) crystal structure, as studied in detail in our previous work.[15]

Figure 1 shows the scattering patterns in the presence of chlorides (panel e) and in the absence of chlorides (panel b), 12 min after the temperature had reached 230 °C. The most prominent feature of in situ scattering patterns in the presence of chlorides is a structure factor peak at $q = 1.45$ nm^{-1} (4.35 nm in real space) arising from stacked nanosheets in solution (Figure 1e). In the absence of chlorides, a structure factor peak is not present, but a plateau is observed with a first minimum at 1 nm^{-1} (Figure 1b). The patterns can be accurately fitted to simple models (solid lines in Figure 1b,e; see Supporting Information, Methods 1 and 2 and Figure S3). The spheroidal nanocrystals obtained in the absence of chlorides are modeled as polydisperse spheres with mean radius R (Figure 1c). The low-q ($<2 \times 10^{-2}$ nm^{-1}) scattering is ascribed to self-organization of nanocrystals into superstructures (see Figure 1b and Supporting Information, Method 2). The stacks of nanosheets are modeled as platelets with thickness $h = 2$ nm (determined from TEM) and circular cross-section of polydisperse diameter D, with inter-NS stacking distance d and a distributed number N of platelets per stack with total length L (Figure 1f and Supporting Information, Method 1 and Figure S3).

Formation of Spheroidal Colloidal $Cu_{2-x}S$ Nanocrystals. Supramolecular species and metal–organic frameworks, such as the copper–alkylthiolates used in this work, have emerged as single-source precursors for synthesis of semiconductor nanocrystals by thermolysis.[32−35] Copper–alkylthiolates are known to form a lamellar phase, which melts into a columnar mesophase at low temperatures (143.5 °C for Cu–DDT) and an isotropic liquid at higher temperatures (205.6 °C for Cu–DDT).[30] In SAXS experiments, these ordered lamellar phases should give rise to structure factor peaks at large q values (between 1 and 2 nm^{-1}), allowing their existence to be monitored in real time. Indeed, our in situ SAXS experiments show one set of structure factor peaks at regular intervals for the reaction in the absence of chlorides (Figure 2a). From the structure factor peak positions, the interlamellae separation is deduced ($2\pi/q = 3.6$ nm), consistent with reported values for stacks of Cu–DDT lamellar complexes.[30] At 150 °C, the structure factor peaks disappear, indicating that the lamellar structure melts. We find no evidence for the presence of a liquid columnar mesophase. It is likely that the columnar mesophase is not stable when the Cu–DDT complex is diluted in a solvent (ODE in this case), and instead an isotropic solution is formed. After nucleation ($T = 230$ °C, evidenced by a color change from yellow to brown), a broad scattering signal is observed with minimum scattering intensity around 3 nm^{-1} (yellow line in Figure 2b). The minimum in scattering intensity moves toward smaller q values over time, indicating growth of nanocrystals (Figure 2b). This is form factor scattering typical for nearly spherical nanocrystals,[31,36,37] consistent with the TEM images in Figure 1. The scattering patterns were fitted to the form factor of polydisperse spheres, from which the growth in diameter of the nanocrystals is obtained (Figure 2c and Supporting Information, Method 2). We find that the mean diameter of the nanocrystals increases from 1 nm to a final value of 8 nm over 17 min.

The formation of colloidal nanocrystals can proceed by three different regimes: monomer-, diffusion-, or reaction-limited.[38−40] In the first regime, the rate-limiting step is conversion of precursors to monomers, which limits both nucleation and growth rates. In the second regime, monomer formation and NC nucleation are faster than diffusion of monomers to the NC surface, which thus becomes the rate-limiting step for NC growth. In the reaction-limited regime, growth rates are limited by the incorporation of monomers into growing nanocrystals. The temporal evolution of the average diameter of spheroidal $Cu_{2-x}S$ nanocrystals (Figure 2c) cannot

DOI: 10.1021/acs.chemmater.6b02787
Chem. Mater. 2016, 28, 6381−6389

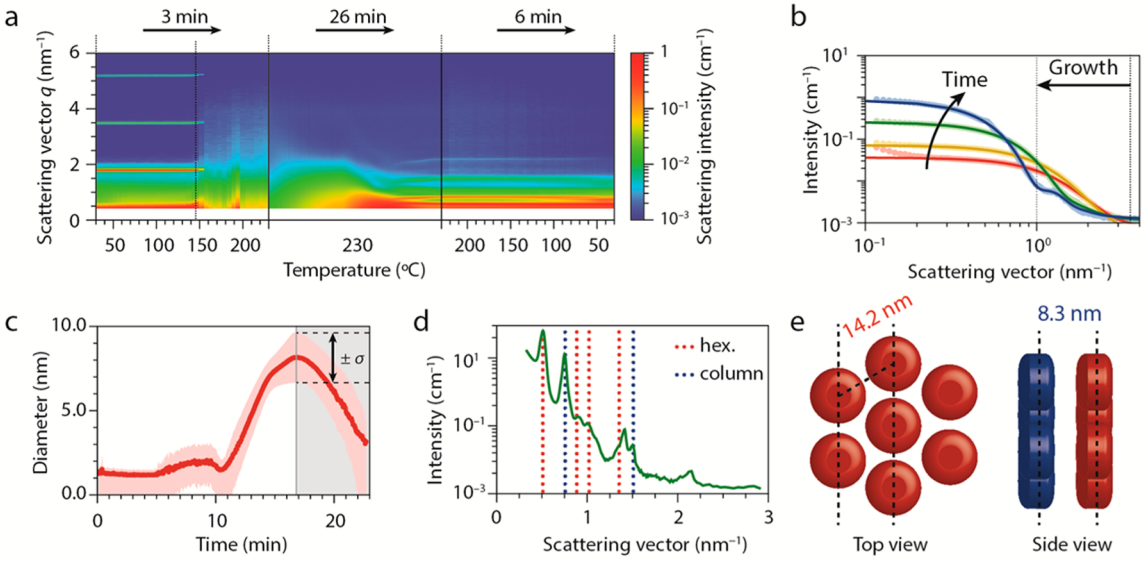

Figure 2. SAXS during formation of spheroidal $Cu_{2-x}S$ nanocrystals. (a) SAXS structure factor peaks of lamellar copper−thiolate precursors (below 150 °C) and form factor scattering of $Cu_{2-x}S$ nanocrystals (at 230 °C), followed over the course of the entire experiment. (b) Four representative SAXS patterns (data points) with their corresponding fits (solid lines), showing close agreement between experiment and model. (c) The nanocrystals grow over time to a final size of ∼8 nm in diameter, in good agreement with the size observed by ex situ TEM measurements (∼9 nm). The shaded area after t = 17 min denotes the period in which the nanocrystals form ordered 3D superstructures, which disrupts the fits to determine NC diameter. (d) After 17 min of growth, the nanocrystals form ordered 3D superstructures, consistent with ex situ TEM observations (Figure 1a). The pattern matches that of a columnar phase formed by hexagonally packed columns of stacked nanocrystals with a stacking distance of 8.3 nm (blue dotted lines), and an intercolumn separation of 14.2 nm (red dotted lines). (e) Schematic of top and side views of columnar superstructure, indicating the separation between the nanocrystals (8.3 nm) within the plane as well as between the columns (14.2 nm).

be precisely described by either the reaction- or diffusion-limited growth model (Supporting Information, Method 3 and Figure S4). Moreover, a reasonable fit can be obtained only if an induction period of 10.9 min is included prior to the onset of nucleation and growth. During the induction period, the average diameter of the scattering species remains constant at 1.44 nm, while the total scattering volume increases with time (Supporting Information, Figures S4 and S5). This suggests that the scattering species are [CuS] monomers or subcritical nuclei that are being formed by thermolysis of copper−dodecanethiolate precursors and are slowly accumulating in the reaction medium until the critical nucleation threshold is reached. Induction periods are often observed in the synthesis of colloidal nanocrystals,[1,39] indicating that the rate-limiting step is the precursor to monomer conversion.[1,29,39] Our results thus show that formation of $Cu_{2-x}S$ spheroidal nanocrystals from copper−dodecanethiolate precursors is limited by monomer formation rates, which are in turn dictated by thermolysis of the C−S bonds of the precursors. This is in line with the model previously proposed by Iversen and co-workers.[24]

After 17 min of growth at 230 °C, sharp peaks appear in the SAXS pattern (Figure 2a,d), which can be ascribed to structure factor peaks of an ordered superstructure, formed by self-organization of the nanocrystals. The structure factor peaks can be matched to a columnar structure of nanocrystals (Figure 2e). The slightly oblate nanocrystals are stacked face-to-face in columns (blue dotted lines in Figure 2d, stacking distance 8.3 nm), with the columns in hexagonal order[41−43] (red dotted lines in Figure 2d, inter-NC separation 14.2 nm). The three-dimensional (3D) ordered superstructure of oblate nanocrystals remains intact when the reaction mixture is cooled down to room temperature, as evidenced by the preservation of the structure factor peaks. Indeed, ordered NC superstructures were observed with ex situ TEM after the reaction had reached completion (see Figure 1a).

Formation of Ultrathin Colloidal $Cu_{2-x}S$ Nanosheets. We now discuss the precursor decomposition and the nucleation and growth of $Cu_{2-x}S$ in the presence of chlorides, which results in ultrathin colloidal $Cu_{2-x}S$ nanosheets. Figure 3a shows the time evolution of scattering at high q values (0.5−6 nm^{-1}) over the course of the entire experiment. As seen previously, scattering peaks from stacks of lamellar precursor complexes are observed below 150 °C. However, when chlorides are present, there are three sets of peaks originating from lamellar stacks with different interlamellae separations (Figure 3b). Clearly, the presence of chloride alters the structure of the precursor, such that three different lamellar phases appear. Two of those phases melt at 150 °C, but chloride stabilizes one phase (denoted with three asterisks in Figure 3b) beyond the onset of $Cu_{2-x}S$ nucleation at 230 °C (Figure 3c). The red data points in Figure 3c denote the stacking distance of the lamellar precursors as a function of temperature in the presence of chloride.

At the nucleation threshold temperature of 230 °C (evidenced by the color change of the solution inside the capillary from yellow to brown), the remaining stacked precursor phase (denoted by three asterisks, low-intensity peak) directly evolves into $Cu_{2-x}S$ NS stacks (blue line in Figure 3c and sharp peak at q = 1.45 nm^{-1} in Figure 3d, indicated with a blue triangle). Prior to nucleation, the stabilized precursor phase shrinks from a stacking distance of 4.6 nm at 100 °C to 4.0 nm at 230 °C (Figure 3c). This shrinking may be due to reorganization of the thiolate chains but may also indicate the onset of thermolysis of C−S bonds and formation of $Cu_{2-x}S$ nuclei, which would be accompanied by loss of alkyl chains and shortening of the Cu−S bonds and therefore by volume reduction. The structure factor peak

DOI: 10.1021/acs.chemmater.6b02787
Chem. Mater. 2016, 28, 6381−6389

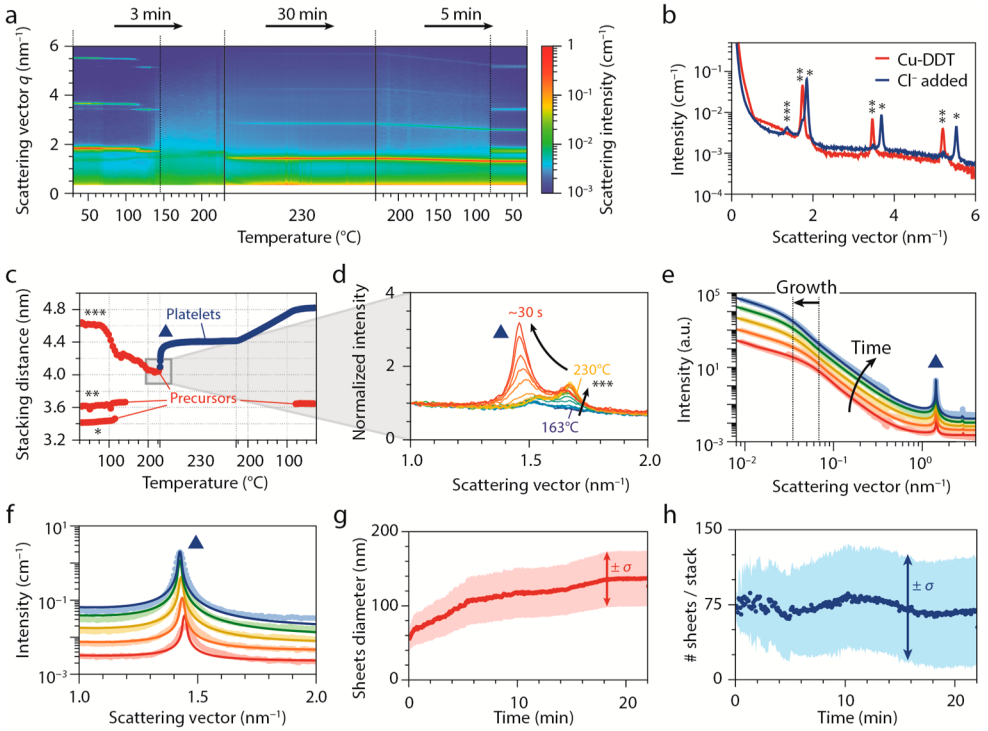

Figure 3. SAXS during the formation of ultrathin $Cu_{2-x}S$ nanosheets. (a) SAXS structure factor peaks of lamellar copper−thiolate precursors (below 150 °C), $Cu_{2-x}S$ NS stacks, and form factor scattering of $Cu_{2-x}S$ nanosheets (above 230 °C) followed over the course of the entire experiment. (b) Snapshots of SAXS patterns at the start of the experiments, showing structure factor peaks associated with lamellar copper−thiolate precursors in the presence of chlorides (blue line) and in the absence of chlorides (red line). Asterisks denote the structure factor peaks and their corresponding overtones. (c) From the position of the stacking peaks in the range $q = 1–2$ nm^{-1}, we deduce the time evolution of the stacking distance of precursor complexes (red) and nanosheets (blue). It can be seen that directly after the nucleation threshold is reached (~230 °C), NS stacks are already present in the reaction medium (blue line, indicated with a blue triangle). (d) Enlarged view of precursor evolution around the nucleation threshold shows a direct transition from the low-intensity precursor peak (q = 1.65 nm^{-1}, denoted with three asterisks) toward the structure factor peak associated with stacking nanosheets (q = 1.45 nm^{-1}, blue triangle). The NS stacking structure factor peak eventually grows in intensity and becomes the only structure factor peak present within the first 30 s after nucleation. (e) Five representative SAXS patterns (data points) with their corresponding fits (solid lines), showing close agreement between experiment and model. The nanosheets grow over time, as indicated by the shift of the transition from q^{-1} dependence to q^{-3} dependence in the SAXS patterns toward smaller q values. (f) Enlarged view of the structure factor peak associated with stacks of nanosheets, showing a small shift to smaller q values (that is, larger inter-NS separation) over the first 30 s. (g) SAXS patterns were fitted with our model (see Supporting Information), from which we deduce the NS diameter and find final lateral dimensions of ~130 nm (σ = 40 nm), consistent with TEM data. (h) From fits of the structure factor peak at q = 1.45 nm^{-1}, the number of nanosheets in a stack is obtained, which remains constant over the course of the entire experiment, at a value of 75 NS/stack.

arising from stacks of nanosheets in solution (at q = 1.45 nm^{-1}, denoted with a blue triangle in Figure 3d) then increases rapidly in intensity, as well as the overtones (see Figure 3a,e). Eventually, they become the only structure factor peaks visible within the first 30 s after nucleation (Figure 3d). After 30 min of growth time, the capillaries were allowed to cool to room temperature, which leads to reappearance of the structure factor peak at q = 1.75 nm^{-1}, indicating that one phase of stacked lamellar copper−thiolate complexes re-forms upon cooling (that is, precursor conversion to $Cu_{2-x}S$ does not reach full yield).

From these high-q measurements, we conclude that the $Cu_{2-x}S$ nanosheets are already stacked when they form at 230 °C, implying that the stacks of chloride-stabilized copper−thiolate lamellae are directly converted to $Cu_{2-x}S$ nanosheets. In other words, the copper−dodecanethiolate precursor lamellae undergo thermolysis while being still structurally intact and stacked, resulting in stack-templated 2D-constrained nucleation and anisotropic growth of $Cu_{2-x}S$ nanosheets (as will be discussed in more detail). The thickness of $Cu_{2-x}S$ nanosheets remains constant throughout the growth period, as evidenced by the fixed position of the NS stacking peak at q = 1.45 nm^{-1}. Lateral growth of the nanosheets was followed by fitting the full scattering patterns with the model introduced above (Figure 1 and also Method 1 in Supporting Information). Figure 3e shows five representative SAXS patterns (data points) and their corresponding fits (solid lines). Figure 3f is an enlarged view of the structure factor peak associated with 1D order of the NS stacks. Using the model, we determine the evolution of NS diameters, assuming a Gaussian distribution with mean diameter D and standard deviation σ. We find that D increases from 60 nm (σ = 15 nm) to 130 nm (σ = 40 nm, Figure 3g) over 22 min. The final fitted diameter is in close agreement with the TEM measurement in Figure 1a (diameter 110 nm). Lateral growth is directly visible from the SAXS patterns in Figure 3e, where a shift of the transition from q^{-1} dependence (10^{-2} to 4×10^{-2} nm^{-1}) to q^{-3} dependence (7×10^{-2} to 7×10^{-1} nm^{-1}) is observed toward smaller q values, indicating growing platelike objects.[31] Meanwhile, the number of nanosheets per stack remains constant at, on average, 75 NS/stack during the entire growth period (Figure 3h). Clearly, the nanosheets are formed directly from the precursor stacks and remain stacked while growing. This stacking is likely the reason for the strongly anisotropic growth, resulting in high

DOI: 10.1021/acs.chemmater.6b02787
Chem. Mater. 2016, 28, 6381−6389

aspect ratio nanosheets (AR = 55), by allowing growth solely in the lateral direction.

We adapted the models describing the diffusion- and reaction-limited growth regimes of spherical nanocrystals to platelike nanocrystals,[29,38−40] and used them to fit the temporal evolution of the lateral dimensions of $Cu_{2-x}S$ nanosheets (Figure 3g and Supporting Information, Figure S6). Similar to the case of spheroidal $Cu_{2-x}S$ nanocrystals discussed previously, both reaction- and diffusion-limited growth models fail to precisely describe our experimental data. Therefore, we conclude that, also in the case of nanosheets, lateral growth is limited by precursor to monomer conversion rates.

It should also be noted that the induction period is absent in growth of the nanosheets, which already have a diameter of 61.8 nm when they are first observed. Interestingly, the total scattering volume starts at nearly 0 at the onset of NS formation and steadily increases over time (Supporting Information, Figure S7). These apparently conflicting observations can be rationalized by considering that the growth of nanosheets has two different stages: very fast initial growth immediately after nucleation, followed by slower growth, which is limited by precursor to monomer conversion rates. This is also supported by the observation that copper−dodecanethiolate lamellar phases that are not chloride-stabilized are not fully consumed and re-form upon cooling of the reaction mixture (Figure 3a,c). Since nucleation is stochastic in nature but growth is deterministic,[1] temporal evolution of the total scattering volume reflects the limits imposed by nucleation rates (both total number of nanosheets and their volume increase over time), while temporal evolution of the lateral size of the nanosheets primarily reflects the constraints imposed by growth rates in the slower growth regime. As will be discussed, this is consistent with the model proposed here, in which stacks of lamellar Cu−DDT are directly converted into stacks of $Cu_{2-x}S$ nanosheets.

Mechanism for Formation of Ultrathin Colloidal $Cu_{2-x}S$ Nanosheets. The results discussed so far show that chlorides increase the thermal stability of stacks of lamellar Cu−DDT complexes while also increasing interlamellar separation from 3.6 to 4.6 nm (Figure 3c). In our previous study,[15] we have shown that halides (Br and Cl) affect both room-temperature morphology and optical spectra of the Cu−DDT precursor. These observations indicate that halides directly coordinate to Cu(I) ions in Cu−DDT lamellar complexes, thereby modifying their properties. Halides may be expected to strongly impact metal−organic frameworks and inorganic coordination polymers based on Cu(I) as connectors, since they are capable of binding as polycoordinated bridging atoms between multiple (up to four) Cu(I) atoms, often forming $[(CuX)L]_n$ coordination polymers (where L= sulfur-donor ligand) with highly variable structures, ranging from 1D to 2D and 3D.[44]

In the present case, we propose that chloride forms polycoordinated bonds with Cu(I) ions in lamellar Cu−DDT complexes, thereby bridging multiple Cu(I) ions and increasing thermal stability of the Cu−DDT framework. This is also consistent with the previously reported observation that $Cu_{2-x}S$ nanosheets contain a significant amount of halides [average Cu/S/halide elemental ratios are $(2.0 \pm 0.2)/1.0/(0.30 \pm 0.06)$].[15] It should be noted that the halides are not replacing the sulfur atoms, since the Cu/S ratio is close to 2, which is consistent with surface-bound halides. The halides are presumed to be randomly distributed over the top and bottom facets of the nanosheets, since their high mobility precluded mapping their exact position by STEM-EDS (scanning transmission electron microscopy−energy-dispersive X-ray spectroscopy).[15] If we take the elemental ratio determined for $Cu_{2-x}S$ nanosheets as a lower limit estimate for the Cu/halide ratio in Cl-modified Cu−DDT lamellar precursor complexes and consider that the $Cu_{2-x}S$ nanosheets are five monolayers thick (2 nm),[15] then the ratio between surface Cu(I) ions and halides would be on average 2.8 ± 0.8. This is consistent with the Cl ions binding as polycoordinated bridging atoms between multiple Cu atoms, as proposed. The exact geometry of the resulting $[Cu_xDDT_yCl]_n$ 2D coordination polymer cannot be determined with the presently available data and is beyond the scope of this paper. However, as demonstrated in our previous work,[15] optical properties of the precursor lamellar Cu−DDT complexes are typical of polynuclear Cu(I) complexes with halides and sulfur-donor ligands,[44,45] thus providing compelling evidence for direct coordination of halides to $Cu_4(DDT)_4$ units. This is further supported by the significant enhancement of photoluminescence quantum yields of lamellar Cu−DDT complexes in the presence of halides, which can be attributed to shorter Cu−Cu distances[45] and restriction of intramolecular rotations,[46] consistent with the formation of a more compact and structurally rigid framework.

The increased thermal stability of Cl-modified Cu−DDT complexes ensures that the structural integrity of lamellar stacks is preserved beyond the onset of Cu-catalyzed thermolysis of the C−S bonds (Figure 4a), leading to two-dimensionally stack-templated nucleation and growth of ultrathin $Cu_{2-x}S$ nanosheets. In the absence of chloride, the stacks of lamellar Cu−DDT complexes disassemble at temperatures below the onset of C−S thermolysis, forming an isotropic liquid. Therefore, when thermolysis starts, [Cu−S] monomers will be produced in solution and will induce homogeneous $Cu_{2-x}S$ nucleation at sufficiently high supersaturations (Figure 4b). Growth then results in the formation of spheroidal $Cu_{2-x}S$ nanocrystals, which eventually self-organize into 3D superstructures.

As discussed, the growth of the nanosheets consist of two different stages: very fast initial growth immediately following nucleation, which results in nanosheets with an average diameter of 61.8 nm within the first tens of seconds of the reaction, followed by slower growth (Figure 3g). The fast initial growth can be understood by considering that thermally induced C−S bond cleavage is catalyzed both by Cu(I) atoms in the copper−dodecanethiolate complex[47] and by specific facets of the $Cu_{2-x}S$ nanocrystals.[32] Therefore, monomer production rates are likely accelerated in the vicinity of the 2D-constrained $Cu_{2-x}S$ nucleus. Since the Cu−DDT lamellae are still intact when C−S thermolysis starts, a high monomer concentration will suddenly become available and will be confined within the boundaries of the chloride-stabilized lamellae. This will lead to a burst of fast radial growth, which is likely self-limited due to the contraction that must accompany formation of $Cu_{2-x}S$ nanocrystals from Cu−DDT precursors, since the alkyl chains are released and the Cu−S bonds shorten. Subsequent growth can then occur only by [Cu−S] monomer addition in the lateral facets, since face-to-face stacking of the chloride-stabilized precursor lamellae inhibits growth in the thickness direction by hindering monomer diffusion and inter-NS mass transport. As a result, the thickness of the nanosheets remains constant throughout

DOI: 10.1021/acs.chemmater.6b02787
Chem. Mater. 2016, 28, 6381−6389

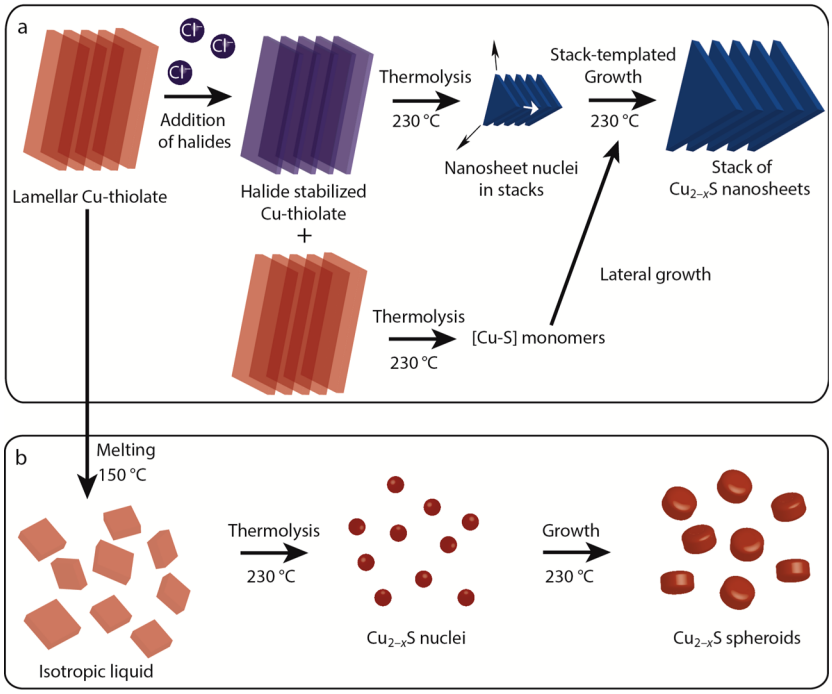

Figure 4. Schematic representation of the formation mechanism of $Cu_{2-x}S$ nanocrystals under different conditions. (a) Formation of ultrathin $Cu_{2-x}S$ nanosheets. Stacks of lamellar copper−thiolate precursors, in the presence of coordinating chloride ions, are stabilized to temperatures above the nucleation threshold. After thermolysis of C−S bonds, this results in 2D-constrained stack-templated nucleation of $Cu_{2-x}S$ nanosheet. (b) Formation of spheroidal $Cu_{2-x}S$ nanocrystals. In the absence of chloride, the lamellar copper−thiolate complexes melt and form an isotropic liquid, which after C−S thermolysis produces free Cu−S monomers in solution, eventually resulting in nucleation and growth of spheroidal $Cu_{2-x}S$ nanocrystals.

the growth process, while the lateral dimensions increase by addition of [Cu−S] monomers from the growth solution. Growth rates in the slow-growth stage thus become limited by precursor to monomer conversion rates.

Typically, the limited growth in thickness of colloidal 2D nanosheets is ascribed to surface ligands and soft-templating effects.[9−11,48] Our approach bears similarities with the soft-templating mechanisms previously proposed, since the stacked lamellar precursors act as a soft template that not only directs the initial nucleation and growth of ultrathin $Cu_{2-x}S$ nanosheets but also prevents subsequent increase in thickness, while allowing lateral growth to continue. Our work provides the first direct observation of a soft template and also the first evidence of NS stacking as a thickness-determining mechanism, leading to formation of ultrathin nanosheets with well-defined thickness (viz., 2 nm). Our approach of adding stabilizing agents to lamellar metal−sulfide complexes may be further exploited to produce nanosheets of various metal sulfide compositions, by taking advantage of the rich library of lamellar M−thiolate complexes currently available (with M = Fe, Ni, Cu, Co, Cd, Zn, Pd, Pt, Ag, Au, Pb, and Bi)[49−54] and the availability of polycoordinating bridging species (such as chloride in this work). Moreover, as demonstrated in our previous work,[15] different halides lead to different NS shapes (Br, hexagonal; Cl, triangular), and the NS composition can be postsynthetically tailored by use of topotactic cation-exchange reactions.

CONCLUSIONS

In conclusion, our in situ SAXS study reveals the stack-templated formation mechanism of complex multiscale nucleation and growth of 2D colloidal $Cu_{2-x}S$ nanosheets. We show that chloride forms direct bonds with lamellar copper−thiolate complexes, which ensures that their structural integrity remains intact beyond the onset of $Cu_{2-x}S$ nucleation. We effectively followed the lamellar copper−thiolate precursor transformations and the size and shape evolution of 2D colloidal $Cu_{2-x}S$ nanosheets via in situ SAXS at three detector-to-sample distances. Our results show that lamellar stacks of copper−thiolate precursor complexes melt into an isotropic liquid around 150 °C in the absence of chloride but persist until above the nucleation threshold (230 °C) in the presence of chlorides. In this way, Cu-catalyzed thermolysis of the C−S bond results in 2D-constrained stack-templated nucleation and growth of $Cu_{2-x}S$ nanosheets. Stacking of the nanosheets precludes growth in the thickness direction, thereby effectively limiting the thickness to 2 nm. Furthermore, we find that lateral growth of colloidal 2D $Cu_{2-x}S$ nanosheets is mainly limited by the slow precursor to monomer conversion. Our work provides important insights into the formation of 2D nanomaterials from lamellar copper−thiolate complexes and may prove beneficial for the design of synthetic strategies for other 2D metal sulfide nanosheets by deploying metal−thiolate lamellar complexes as precursors.

ASSOCIATED CONTENT

Supporting Information

The Supporting Information is available free of charge on the ACS Publications website at DOI: 10.1021/acs.chemmater.6b02787.

Additional text and equations and six figures showing experimental setup at beamline ID02, ESRF, Grenoble; PXRD and WAXS patterns; cross-section form factor; SAXS models used to fit data; and growth models used

DOI: 10.1021/acs.chemmater.6b02787
Chem. Mater. 2016, 28, 6381−6389

to fit temporal evolution of sizes of both spheroidal nanocrystals and ultrathin nanosheets (PDF)

AUTHOR INFORMATION

Corresponding Author

*E-mail c.demello-donega@uu.nl.

Author Contributions

The manuscript was written through contributions of all authors. All authors have given approval to the final version of the manuscript.

Notes

The authors declare no competing financial interest.

ACKNOWLEDGMENTS

W.v.d.S. and C.d.M.D. acknowledge financial support from the division of Chemical Sciences (CW) of The Netherlands Organization for Scientific Research (NWO) under Grant ECHO.712.012.001. The European Synchroton Radiation Facility (ESRF), Grenoble, France, is acknowledged for the granted beam time under Proposal CH-4389. We thank Giuseppe Portale and Daniel Hermida Merino from the DUBBLE beamline at ESRF for their technical assistance with exploratory measurements, which were supported by NWO under Grant 195.068.854.

REFERENCES

(1) Donega, C. d. M. Synthesis and Properties of Colloidal Heteronanocrystals. *Chem. Soc. Rev.* **2011**, *40*, 1512−1546.

(2) Murray, C. B.; Norris, D. J.; Bawendi, M. G. Synthesis and Characterization of Nearly Monodisperse CdE (E= S, Se, Te) Semiconductor Nanocrystallites. *J. Am. Chem. Soc.* **1993**, *115*, 8706−8715.

(3) Carbone, L.; Nobile, C.; De Giorgi, M.; Della Sala, F.; Morello, G.; Pompa, P.; Hytch, M.; Snoeck, E.; Fiore, A.; Franchini, I. R.; et al. Synthesis and Micrometer-Scale Assembly of Colloidal CdSe/CdS Nanorods Prepared by a Seeded Growth Approach. *Nano Lett.* **2007**, *7*, 2942−2950.

(4) Ithurria, S.; Tessier, M. D.; Mahler, B.; Lobo, R. P. S. M.; Dubertret, B.; Efros, Al. L. Colloidal Semiconductor Nanoplatelets with Two Dimensional Electronic Structure and Ultrafast Fluorescence Lifetime. *Nat. Mater.* **2011**, *10*, 936−941.

(5) Chhowalla, M.; Shin, H. S.; Eda, G.; Li, L.-J.; Loh, K. P.; Zhang, H. The Chemistry of Two-Dimensional Layered Transition Metal Dichalcogenide Nanosheets. *Nat. Chem.* **2013**, *5*, 263−275.

(6) Wu, X.-J.; Huang, X.; Liu, J.; Li, H.; Yang, J.; Li, B.; Huang, W.; Zhang, H. Two-Dimensional CuSe Nanosheets with Microscale Lateral Size: Synthesis and Template-Assisted Phase Transformation. *Angew. Chem., Int. Ed.* **2014**, *53*, 5083−5087.

(7) Lhuillier, E.; Pedetti, S.; Ithurria, S.; Nadal, B.; Heuclin, H.; Dubertret, B. Two-Dimensional Colloidal Metal Chalcogenides Semiconductors: Synthesis, Spectroscopy, and Applications. *Acc. Chem. Res.* **2015**, *48*, 22−30.

(8) Zhang, H. Ultrathin Two-Dimensional Nanomaterials. *ACS Nano* **2015**, *9*, 9451−9469.

(9) Bouet, C.; Tessier, M. D.; Ithurria, S.; Mahler, B.; Nadal, B.; Dubertret, B. Flat Colloidal Semiconductor Nanoplatelets. *Chem. Mater.* **2013**, *25*, 1262−1271.

(10) Schliehe, C.; Juarez, B. H.; Pelletier, M.; Jander, S.; Greshnykh, D.; Nagel, M.; Meyer, A.; Foerster, S.; Kornowski, A.; Klinke, C.; Weller, H. Ultrathin PbS Sheets by Two-Dimensional Oriented Attachment. *Science* **2010**, *329*, 550−553.

(11) Morrison, P. J.; Loomis, R. A.; Buhro, W. E. Synthesis and Growth Mechanism of Lead Sulfide Quantum Platelets in Lamellar Mesophase Templates. *Chem. Mater.* **2014**, *26*, 5012−5019.

(12) Liu, X.; Li, Y.; Zhou, B.; Wang, X.; Cartwright, A. N.; Swihart, M. T. Shape-Controlled Synthesis of SnE (E = S, Se) Semiconductor Nanocrystals for Optoelectronics. *Chem. Mater.* **2014**, *26*, 3515−3521.

(13) Vaughn, D.; In, S.; Schaak, R. A. Precursor-Limited Nanoparticle Coalescence Pathway for Tuning the Thickness of Laterally-Uniform Colloidal Nanosheets: the Case of SnSe. *ACS Nano* **2011**, *5*, 8852−8860.

(14) Park, K. H.; Jang, K.; Son, S. U. Synthesis, Optical Properties, and Self-Assembly of Ultrathin Hexagonal In_2S_3 Nanoplates. *Angew. Chem., Int. Ed.* **2006**, *45*, 4608−4612.

(15) van der Stam, W.; Akkerman, Q. A.; Ke, X.; van Huis, M. A.; Bals, S.; Donega, C. d. M. Solution-Processable Ultrathin Size-and Shape-Controlled Colloidal $Cu_{2-x}S$ Nanosheets. *Chem. Mater.* **2015**, *27*, 283−291.

(16) Yi, L.; Gao, M. From Ultrathin Two-Dimensional Djurleite Nanosheets to One-Dimensional Nanorods Comprised of Djurleite Nanoplates: Synthesis, Characterization, and Formation Mechanism. *Cryst. Growth Des.* **2011**, *11*, 1109−1116.

(17) Mahler, B.; Hoepfner, V.; Liao, K.; Ozin, G. Colloidal Synthesis of 1T-WS_2 and 2H-WS_2 Nanosheets: Applications for Photocatalytic Hydrogen Evolution. *J. Am. Chem. Soc.* **2014**, *136*, 14121−14127.

(18) Li, Z.; Peng, X. Size/Shape-Controlled Synthesis of Colloidal CdSe Quantum Disks: Ligand and Temperature Effects. *J. Am. Chem. Soc.* **2011**, *133*, 6578−6586.

(19) Yang, J.; Son, J. S.; Yu, J. H.; Joo, J.; Hyeon, T. Advances in the Colloidal Synthesis of Two-Dimensional Semiconductor Nanoribbons. *Chem. Mater.* **2013**, *25*, 1190−1198.

(20) Liu, Y. H.; Wang, F. D.; Wang, Y. Y.; Gibbons, P. C.; Buhro, W. E. Lamellar Assembly of Cadmium Selenide Nanoclusters into Quantum Belts. *J. Am. Chem. Soc.* **2011**, *133*, 17005−17013.

(21) Son, J. S.; Park, K.; Kwon, S. G.; Yang, J.; Choi, M. K.; Kim, J.; Yu, J. H.; Joo, J.; Hyeon, T. Dimension-Controlled Synthesis of CdS Nanocrystals: from 0D Quantum Dots to 2D Nanoplates. *Small* **2012**, *8*, 2394−2402.

(22) Liao, H.-G.; Zherebetskyy, D.; Xin, H.; Czarnik, C.; Ercius, P.; Elmlund, H.; Pan, M.; Wang, L.-W.; Zheng, H. Facet Development During Platinum Nanocube Growth. *Science* **2014**, *345*, 916−919.

(23) Liao, H.-G.; Cui, L.; Whitelam, S.; Zheng, H. Real-Time Imaging of Pt_3Fe Nanorod Growth in Solution. *Science* **2012**, *336*, 1011−1014.

(24) Nørby, P.; Johnsen, S.; Iversen, B. B. In Situ X-ray Diffraction Study of the Formation, Growth, and Phase Transition of Colloidal $Cu_{2-x}S$ nanocrystals. *ACS Nano* **2014**, *8*, 4295−4303.

(25) Søndergaard, M.; Dalgaard, K. J.; Bøjesen, E. D.; Wonsyld, K.; Dahl, S.; Iversen, B. B. In Situ Monitoring of TiO_2(B)/Anatase Nanoparticle Formation and Application in Li-Ion and Na-Ion Batteries. *J. Mater. Chem. A* **2015**, *3*, 18667−18674.

(26) Gordon, T. R.; Diroll, B. T.; Paik, T.; Doan-Nguyen, V. V. T.; Gaulding, E. A.; Murray, C. B. Characterization of Shape and Monodispersity of Anisotropic Nanocrystals through Atomistic X-ray Scattering Simulation. *Chem. Mater.* **2015**, *27*, 2502−2506.

(27) Abécassis, B.; Bouet, C.; Garnero, C.; Constantin, D.; Lequeux, N.; Ithurria, S.; Dubertret, B.; Pauw, B. R.; Pontoni, D. Real-Time *In Situ* Probing of High-Temperature Quantum Dots Solution Synthesis. *Nano Lett.* **2015**, *15*, 2620−2626.

(28) Adachi, M.; Nakagawa, K.; Sago, K.; Murata, Y.; Nishikawa, Y. Formation of GeO_2 Nanosheets Using Water Thin Layers in Lamellar Phase as a Confined Reaction Field − *In Situ* Measurement of SAXS by Synchroton Radiation. *Chem. Commun.* **2005**, 2381−2383.

(29) Wang, Z.; Schliehe, C.; Wang, T.; Nagaoka, Y.; Cao, Y. C.; Bassett, W. A.; Wu, H.; Fan, H.; Weller, H. Deviatoric Stress Driven Formation of Large Single-Crystal PbS Nanosheet from Nanoparticles and In-Situ Monitoring of Oriented Attachment. *J. Am. Chem. Soc.* **2011**, *133*, 14484−14487.

(30) Espinet, P.; Lequerica, M. C.; Martín-Alvarez, J. M. Synthesis, Structural Characterization and Mesogenic Behavior of Copper (I) n-Alkylthiolates. *Chem. - Eur. J.* **1999**, *5*, 1982−1986.

DOI: 10.1021/acs.chemmater.6b02787
Chem. Mater. 2016, 28, 6381−6389

(31) Renaud, G.; Lazzari, R.; Leroy, F. Probing Surface and Interface Morphology with Grazing Incidence Small Angle X-Ray Scattering. *Surf. Sci. Rep.* **2009**, *64*, 255−380.
(32) Larsen, T. H.; Sigman, M.; Ghezelbash, A.; Doty, R. C.; Korgel, B. A. Solventless Synthesis of Copper Sulfide Nanorods by Thermolysis of a Single Source Thiolate-Derived Precursor. *J. Am. Chem. Soc.* **2003**, *125*, 5638−5639.
(33) Chen, L.; Chen, Y.-B.; Wu, L.-M. Synthesis of Uniform Cu_2S Nanowires from Copper-Thiolate Polymer Precursors by a Solventless Thermolytic Method. *J. Am. Chem. Soc.* **2004**, *126*, 16334−5.
(34) Sigman, M.; Ghezelbash, A.; Hanrath, T.; Saunders, A. E.; Lee, F.; Korgel, B. A. Solventless Synthesis of Monodisperse Cu_2S Nanorods, Nanodisks, and Nanoplatelets. *J. Am. Chem. Soc.* **2003**, *125*, 16050−16057.
(35) Wang, Y.; Hu, Y.; Zhang, Q.; Ge, J.; Lu, Z.; Hou, Y.; Yin, Y. One-Pot Synthesis and Optical Property of Copper(I) Sulfide Nanodisks. *Inorg. Chem.* **2010**, *49*, 6601−6608.
(36) Murray, C. B.; Kagan, C.; Bawendi, M. G. Self-Organization of CdSe Nanocrystallites into Three-Dimensional Quantum Dot Superlattices. *Science* **1995**, *270*, 1335−1338.
(37) Guinier, A.; Fournet, G. *Small-Angle Scattering of X-rays*; Wiley: New York, 1955.
(38) Talapin, D. V.; Rogach, A. L.; Haase, M.; Weller, H. Evolution of an Ensemble of Nanoparticles in a Colloidal Solution: Theoretical Study. *J. Phys. Chem. B* **2001**, *105*, 12278−12285.
(39) Rempel, J. Y.; Bawendi, M. G.; Jensen, K. F. Insights into the Kinetics of Semiconductor Nanocrystal Nucleation and Growth. *J. Am. Chem. Soc.* **2009**, *131*, 4479−4489.
(40) Bullen, C. R.; Mulvaney, P. Nucleation and Growth Kinetics of CdSe Nanocrystals in Octadecene. *Nano Lett.* **2004**, *4*, 2303−2307.
(41) Pietra, F.; Rabouw, F. T.; Evers, W. H.; Byelov, D. V.; Petukhov, A. V.; Donega, C. d. M.; Vanmaekelbergh, D. Semiconductor Nanorod Self-Assembly at the Liquid/Air interface Studied by In Situ GISAXS and Ex Situ TEM. *Nano Lett.* **2012**, *12*, 5515−5523.
(42) van der Stam, W.; Rabouw, F. T.; Vonk, S. J. W.; Geuchies, J. J.; Ligthart, H.; Petukhov, A. V.; Donega, C. d. M. Oleic Acid-Induced Atomic Alignment of ZnS Polyhedral Nanocrystals. *Nano Lett.* **2016**, *16*, 2608−2614.
(43) Heitsch, A. T.; Patel, R. N.; Goodfellow, B. W.; Smilgies, D.-M.; Korgel, B. A. GISAXS Characterization of Order in Hexagonal Monolayers of FePt Nanocrystals. *J. Phys. Chem. C* **2010**, *114*, 14427−14432.
(44) Lapprand, A.; Bonnot, A.; Knorr, M.; Rousselin, Y.; Kubicki, M. M.; Fortin, D.; Harvey, P. D. Formation of an Unprecedented $(CuBr)_5$ Cluster and a Zeolite-Type 2D-Coordination Polymer: a Surprising Halide Effect. *Chem. Commun.* **2013**, *49*, 8848−8850.
(45) Ford, P. C.; Cariati, E.; Bourassa, J. Photoluminescence Properties of Multinuclear Copper(I) Compounds. *Chem. Rev.* **1999**, *99*, 3625−3648.
(46) Kang, X.; Wang, S.; Song, Y.; Jin, S.; Sun, G.; Yu, H.; Zhu, M. Bimetallic Au_2Cu_6 Nanoclusters: Strong Luminescence Induced by the Aggregation of Copper(I) Complexes with Gold(0) Species. *Angew. Chem., Int. Ed.* **2016**, *55*, 3611−3614.
(47) Wang, L.; He, W.; Yu, Z. Transition-Metal Mediated Carbon−Sulfur Bond Activation and Transformations. *Chem. Soc. Rev.* **2013**, *42*, 599−621.
(48) Wang, F.; Wang, Y.; Liu, Y.-H.; Morrison, P. J.; Loomis, R. A.; Buhro, W. E. Two-Dimensional Semiconductor Nanocrystals: Properties, Templated Formation, and Magic-Size Nanocluster Intermediates. *Acc. Chem. Res.* **2015**, *48*, 13−21.
(49) Zhuang, Z.; Lu, X.; Peng, Q.; Li, Y. A Facile "Dispersion-Decomposition" Route to Metal Sulfide Nanocrystals. *Chem. - Eur. J.* **2011**, *17*, 10445−10452.
(50) Busupalli, B.; Kummara, S.; Kumaraswamy, G.; Prasad, B. L. V. Ultrathin Sheets of Metal or Metal Sulfide from Molecularly Thin Sheets of Metal Thiolates in Solution. *Chem. Mater.* **2014**, *26*, 3436−3442.
(51) Xu, C.; Zeng, Y.; Rui, X.; Xiao, N.; Zhu, J.; Zhang, W.; Chen, J.; Liu, W.; Tan, H.; Hng, H. H.; et al. Controlled Soft-Template Synthesis of Ultrathin C@FeS Nanosheets with High-Li-Storage Performance. *ACS Nano* **2012**, *6*, 4713−4721.
(52) Wu, W.-Y.; Chakrabortty, S.; Chang, C. K. L.; Guchhait, A.; Lin, M.; Chan, Y. Promoting 2D Growth in Colloidal Transition Metal Sulfide Semiconductor Nanostructures via Halide Ions. *Chem. Mater.* **2014**, *26*, 6120−6126.
(53) Wang, Y.; Tang, A.; Li, K.; Yang, C.; Wang, M.; Ye, H.; Hou, Y.; Teng, F. Shape-Controlled Synthesis of PbS Nanocrystals via a Simple One-Step Process. *Langmuir* **2012**, *28*, 16436−16443.
(54) Chen, J.; Wu, L. M.; Chen, L. Syntheses and Characterizations of Bismuth Nanofilms and Nanorhombuses by the Structure-Controlling Solventless Method. *Inorg. Chem.* **2007**, *46*, 586−591.

DOI: 10.1021/acs.chemmater.6b02787
Chem. Mater. 2016, 28, 6381−6389